
Porous polymer/bioactive glass composites for soft-to-hard tissue interfaces

Kai Zhang, Yue Ma, Lorraine F. Francis

Department of Chemical Engineering and Materials Science, University of Minnesota, 421 Washington Avenue SE, Minneapolis, Minnesota 55455

Received 13 April 2001; revised 18 December 2001; accepted 15 January 2002

Abstract: Porous composites consisting of a polysulfone (or cellulose acetate) matrix and bioactive glass particles were prepared by phase separation techniques. Microstructures were designed for potential application as an interconnect between artificial cartilage and bone. The effects of polymer type, concentration and molecular weight, as well as bioactive glass size and content, on the microstructures of the composites were studied. The composites have asymmetric structures with dense top layers and porous structures beneath. The microstructural features depend most strongly on the type of polymer, the interaction between the polymer and bioactive glass, and the glass content. The dense top layer could be removed by abrasion to make a

structure with large pores (20–150 μm) exposed. Composites were immersed in simulated body fluid at body temperature. The growth of hydroxycarbonate apatite inside and on the composites demonstrates their potential for integration with bone. Composite modulus and break strength increased with increasing glass content due to the change in composition and pore content. © 2002 Wiley Periodicals, Inc. *J Biomed Mater Res* 61: 551–563, 2002

Key words: porous composites; polymer scaffold; bioactive glass; soft-to-hard tissue interface; apatite

INTRODUCTION

The structures and compositions of the interfaces between soft and hard tissue are complex and well designed for their functions.^{1–3} The interface between cartilage and bone, the zone of calcified cartilage (ZCC), serves as a good example.^{1,4} The ZCC extends from the interface between uncalcified cartilage and calcified cartilage (the tidemark) to the interface between calcified cartilage and subchondral bone (the cement line). As the interface attaching cartilage to bone, the ZCC also transfers compressive force and controls the diffusion of tissue fluid containing oxygen and nutrients from bone to other layers of cartilage.⁴ Artificial tissues are needed to perform the function of interfaces such as the ZCC.

Biomaterials and artificial tissues have been developed for soft and hard tissue applications.⁵ For example, the relatively simple structure of cartilage makes the engineering of an artificial cartilage an at-

tractive possibility for repair of damaged cartilage.^{6–10} Autologous chondrocyte transplantation¹¹ and implantation of artificial matrices with cells and growth factors^{7–10,12} are particularly promising because they lead to development of hyaline cartilage. However, developing the interface between the artificial cartilage and the underlying bone presents a challenge. The integration between artificial cartilage and host tissue is poor.^{12,13} Although methods such as sewing and press fitting^{14,15} have been used to integrate artificial cartilage and host tissue, problems still exist for larger defects and long-term application. Also, the interface, the zone of calcified cartilage, is difficult to develop directly from artificial cartilage and natural bone.¹⁶ New methods designed specifically for connecting artificial cartilage and bone are needed.

One strategy is to construct an interface material capable of bonding to both artificial cartilage and bone. Porous polymer/bioactive ceramic composites are candidate materials for engineering the artificial cartilage/bone interface and possibly other soft-to-hard tissue interfaces. A porous polymer matrix with large (>100 μm) pores and small (<10 μm) interconnected pores provides biological bonding via cell attachment and ingrowth and fluid transfer, respectively. The polymer matrix also provides flexibility

Correspondence to: L. F. Francis; e-mail: lfrancis@tc.umn.edu

Contract grant sponsor: MRSEC program of the National Science Foundation; contract grant number: DMR-9809364

and toughness. The bioactive ceramic helps to encourage bonding to bone¹⁷ and may influence calcification in the cartilage.¹⁸ Although research has shown that dense polymer/bioactive glass composites have *in vitro* and *in vivo* bone bonding ability,^{19–21} little attention has been given to the preparation or properties of porous polymer/bioactive glass composites.²²

The choice of polymer and ceramic for the porous composite requires the consideration of the mechanical stability, biocompatibility, and tissue-bonding ability. Biodegradable polymers are candidates for polymer phase,¹⁵ but challenges in developing adequate mechanical properties²³ and controlled degradation still exist.²⁴ A nonbiodegradable biopolymer has advantages such as good mechanical properties and stability.^{25–27} As a nonbiodegradable polymer, polysulfone has good mechanical properties, biocompatibility, and hemocompatibility; in addition, it also has been tested as an orthopedic implant material.^{25,28} Furthermore, techniques to develop porosity in polysulfone are well developed for its application as a membrane.²⁹ For the ceramic phase, bioactive glass bonds well with both hard and soft tissues by the development of a hydroxycarbonate apatite (HCA) layer.^{17,30–33} Bioactive glasses and glass ceramics interact well with osteoblasts and chondrocytes; cells attach, spread, proliferate, and synthesize extracellular matrix on the bioactive glass and glass-ceramic surface.^{18,34} Apatite forms in the presence of bioactive glass particles; thus, it may be possible to control mineralization in the composite by changing the glass content. The incorporation of ceramic particles can also strengthen the porous polymer matrix.

In this work, a phase separation method previously developed in our laboratory^{35,36} was used to form porous polymer/bioactive glass composite. A homogeneous polymer solution containing ceramic particles was separated into polymer/ceramic-rich phase and polymer-lean phases by changing the polymer solubility through solvent (or nonsolvent) composition changes. The final microstructure contains a continuous structure resulting from polymer/ceramic-rich phase and pores from the drying of polymer-lean phase. Microstructures are affected by the interaction between the polymer and the ceramic as well as the ceramic particle size and content.^{35,36} Composites with both large open pores (size >100 μm) and interconnected small pores (size <5 μm) can be prepared. This report focuses on the phase separation processing and morphologies of the porous polymer/bioactive glass composites. The effects of polymer choice, as well as glass particle size and content on microstructure, are explored, some mechanical properties are characterized, and *in vitro* growth HCA inside and on the composites are studied.

MATERIALS AND METHODS

Materials

Polysulfone ($M_w = 35,000$ or $66,000$), cellulose acetate ($M_w = 30,000$), tetrahydrofuran (THF), *N,N*-dimethylacetamide, acetone, and ethanol were obtained from Aldrich Chemical Company. Bioactive glass with a composition of 4.6MgO, 44.7CaO, 34.0SiO₂, 16.2 P₂O₅, and 0.5 CaF₂ (wt%) was purchased from Specialty Glass, Inc. The as-received glass has an average particle size of 9.4 μm and a size distribution from 0.04 to 58 μm as measured by a Coulter® LS 230 Particle Analyzer. Some of the bioactive glass was further processed in an attrition mill to achieve an average particle size of 2.05 μm and a size distribution from 0.04 to 23 μm . The Brunauer–Emmett–Teller (BET) specific surface areas of the as-received and milled glass particles are 1.53 m²/g and 9.79 m²/g, respectively. The glass particles are dense and have an irregular morphology from fracture during size reduction.

Preparation of porous polymer/bioactive glass composites

Polysulfone/bioactive glass composites were prepared by a phase-separation technique based on a method designed for polysulfone membranes,³⁷ which was adapted to include ceramic particles. Homogeneous dispersions were made by dispersing bioactive glass particles in a mixture of THF, DMAc (solvents for polysulfone), and ethanol (a nonsolvent for polysulfone) and then dissolving polysulfone into the glass dispersion. Dispersions with different compositions were prepared (see Table I). Dispersions were cast onto glass substrates by a doctor blade (gap height = 800 μm). The resultant coatings were dried under flowing moist air about 10 s and then immersed with substrate in a water bath for at least 10 min to induce further phase separation. The composites separated from their substrates in the water bath. Then, a solvent exchange³⁷ was performed in methanol. The exchange prevented collapse of the porous structure during drying. The composites were dried at room temperature for at least 24 h and then in a vacuum oven at 70°C for 2 h. Pure polysulfone specimens were also prepared using this method.

The effect of the polymer choice on the composite microstructure was studied by using cellulose acetate as the polymer phase and employing a phase separation technique designed for ceramic/polymer composites.³⁵ Homogeneous dispersions were made by combining cellulose acetate, bioactive glass particles, acetone (a solvent for cellulose acetate), and water (a nonsolvent for cellulose acetate; see Table II). Dispersions were cast onto glass substrates by a doctor blade (gap height = 800 μm), and the resultant coatings and substrates were immediately immersed in a water bath for 10 min to induce phase separation. The composites separated from their substrates in the water bath were dried at room temperature for at least 24 h. Solvent exchange was not necessary.

TABLE I
Polysulfone/Bioactive Glass Composite Compositions

Specimen	Polysulfone:Solvents: Non-solvent (wt. ratio)	Polysulfone Molecular Weight	Glass:Polysulfone (wt. ratio)	Avg. Glass Particle Size (μm)	Glass Vol.% in composite ^a
PS1	14:76:10	35,000	1:4	2.05	9.4
PS2	14:76:10	66,000	1:4	2.05	9.4
PS3	22:63.6:14.4	35,000	1:4	2.05	9.4
PS4	14:76:10	35,000	1:4	9.4	9.4
PS5	14:76:10	35,000	1:1.6	2.05	20.5
PS6	14:76:10	35,000	1:1	2.05	29.2
PS7	14:76:10	35,000	0	N/A	0

^aRelative to total solids.

Interaction between polymers and bioactive glass particles

To better understand the composites' microstructural development, the adsorption of polymer onto bioactive glass particles was studied. Glass dispersions with varying relative amounts of cellulose acetate were prepared by adding 0.1, 0.25, 0.5, 0.75, 1.0, and 1.2 g cellulose acetate to individual dispersions of bioactive glass (1.3g, size = 2.5 μm) in acetone (7.0 g) and water (2.5 g). The individual dispersions were mixed on a stir plate for 24 h and then centrifuged, decanted, and washed with acetone (10.0 g) five times to remove nonadsorbed polymer. The resultant specimens were dried at room temperature. Glass dispersions with varying relative amounts of polysulfone were prepared by adding 0.5, 1.0, 1.4, and 2.0 g polysulfone to individual dispersions of bioactive glass (0.35 g, size = 2.5 μm) in DMAc (3.8 g), THF (3.8 g), and ethanol (1.0 g). The individual dispersions were mixed on a stir plate for 24 h and then centrifuged, decanted, and washed with DMAc (10.0 g) five times. The resultant specimens were dried at room temperature. The weight loss from these specimens was characterized from 30 to 800°C using a Perkin-Elmer TGA-7 thermogravimetric analyzer. The weight losses from polysulfone, cellulose acetate, and bioactive glass powders were also determined for comparison. Results were analyzed to determine the amount of polymer adsorbed on particle surfaces.

Study of HCA growth in simulated body fluid (SBF)

SBF³⁸ has almost the same ion concentrations as that of human blood plasma and serves a medium for *in vitro* investigations of apatite growth. The SBF was prepared by dissolving reagent-grade chemicals NaCl, NaHCO₃, KCl,

K₂HPO₄ · 3H₂O, MgCl₂ · 6H₂O, and CaCl₂ in deionized water in a polypropylene bottle and buffered at pH 7.25 with 50 mM tris(hydroxymethyl) aminomethane [(CH₂OH)₃CNH₂] and 45 mM HCl at 37°C. Composites (1 cm × 1 cm) were soaked individually in 50 mL of SBF at 37°C. Two methods were used in this study: (1) composites were transferred to SBF immediately after the phase separation was finished in the water bath (without drying) and (2) dried composite surfaces were abraded by sand paper (400 grit), immersed in ethanol, and then transferred to SBF. Only method (1) was used for the cellulose acetate/bioactive glass composites. The SBF was changed every other day. After 2 weeks, composites were washed with ethanol and then dried at room temperature for further characterization. Porous polysulfone and cellulose acetate membranes were also soaked by the first procedure.

Composite characterization

Scanning Electron Microscopy (SEM, Hitachi S800 and S900) was used to characterize the microstructure of the composites prepared with different dispersion compositions and after soaking in SBF for 2 weeks. Porosity of some composites was measured by mercury porosimetry (Micromeritics model Poresizer 9320). X-ray diffraction and Fourier transform-infrared spectroscopy patterns of the composites after soaking in SBF were performed on a Bruker-AXS microdiffractometer with 2.2 kW sealed Cu X-ray source and a Nicolet Magna-IR 750 (diffuse reflectance mode, DRIFTS) spectrometer, respectively.

The mechanical tests were performed with a Perkin-Elmer DMA-7 dynamic mechanical analyzer attached to a PC via a DMA7/DX thermal controller. Specimens for mechanical property tests were abraded to remove the dense top surface layers (see procedure above). This process made the speci-

TABLE II
Cellulose Acetate/Bioactive Glass Composite Compositions

Specimen	Cellulose Acetate: Solvent: Non-solvent (wt. ratio)	Glass: Cellulose Acetate (wt. ratio)	Avg. Glass Particle Size (μm)	Glass Vol.% in Composite ^a
CA1	5:70:25	1:0.8	2.05	33.3
CA2	5:70:25	1:0.4	2.05	50.0
CA3	5:70:25	1:0.2	2.05	66.7
CA4	12:63:25	1:0.9	2.05	30.8

^aRelative to total solids.

men thickness more uniform (typical variation $\leq 10\%$). Average thickness values were used for calculation of mechanical properties; the error imparted by this procedure was less than that due to sample-to-sample variation. A static stress mode (loading rate: 500 mN/min) was used for tensile tests. Elastic modulus was calculated from the elastic region (up to 1% strain) of the stress-strain curve. Break strength was also determined. Results are reported for data collected for nine specimens for each material. Statistical analysis of the data was performed using a student's *t* test to determine whether differences exist to a level of significance of $p < 0.05$. The porosity of specimens used for DMA testing was determined from bulk density measurements; data are reported for an average of five specimens.

RESULTS AND DISCUSSION

Microstructures of porous polymer/bioactive glass composites

SEM images of a polysulfone/bioactive glass composite are shown in Figure 1. The average thickness of

the composite was $\sim 300 \mu\text{m}$. The composite thickness was uneven as a result of the preparation method: The drying stage in moist air induced surface ripples that persist in the final structure. This feature can be minimized. The structure consists of a dense polymer-rich layer at the surface that was in contact with the water bath and a porous supporting layer with small and large voids. The size of larger voids is between 20 and $150 \mu\text{m}$. The smaller pores have an average size of $5 \mu\text{m}$ and appear to be interconnected. This porous structure is a characteristic morphology of the polysulfone membranes formed by phase separation.²⁹ The glass particles are well distributed in the composite, on the pore surfaces, and in the polysulfone matrix. Fine, spherical polymer particles ($\sim 200 \text{ nm}$ size) were sometimes found on the composite surface that was in contact with the glass [Fig. 1(d)]. These particles are likely formed by precipitation from the polymer-lean phase during processing.

The effects of changing polysulfone concentration and bioactive glass content and size on the microstruc-

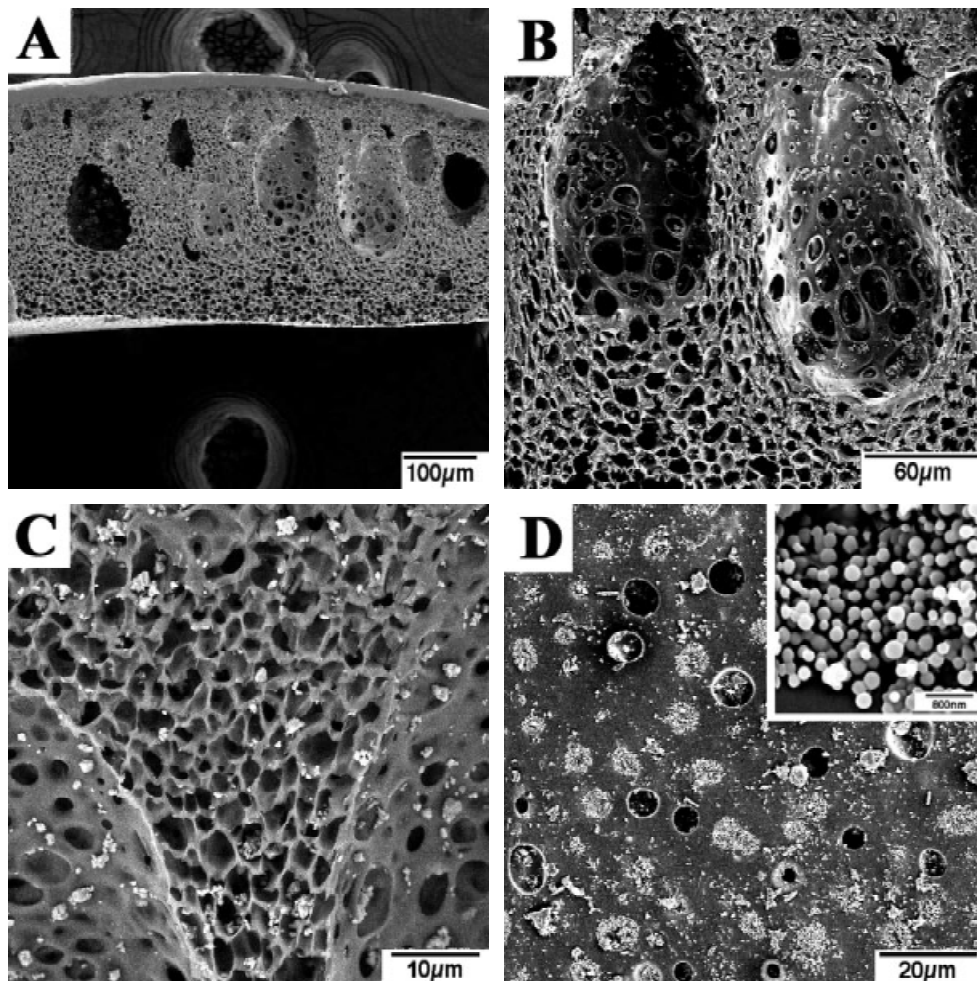


Figure 1. SEM images of porous polysulfone/bioactive glass composite (PS1): (A) cross-section, 150 \times ; (B) cross-section, 400 \times ; (C) cross-section, 1000 \times ; backscattered image which highlights glass particles; (D) bottom surface with inset to show fine polymer particles. Top surface is dense and featureless (not shown).

ture relative to PS1 (Fig. 1) are shown in Figure 2. The microstructures of all composites (see Table I) contained the features described above and are similar to those of polysulfone alone [PS7, Fig. 2(a)]. Increasing the polymer concentration in the dispersion [PS3, Fig. 2(b)] led to a small decrease in the number density of larger voids, but changing the polymer molecular

weight (PS2, not shown) had little effect on the microstructure. When larger glass particles were used [PS4, Fig. 2(c)], again the microstructure is similar but there were fewer particles overall in the composite. With increasing glass content [Fig. 2(d-f)], more particles were apparent, especially on the pore surfaces, but the void structure was not affected much until the highest

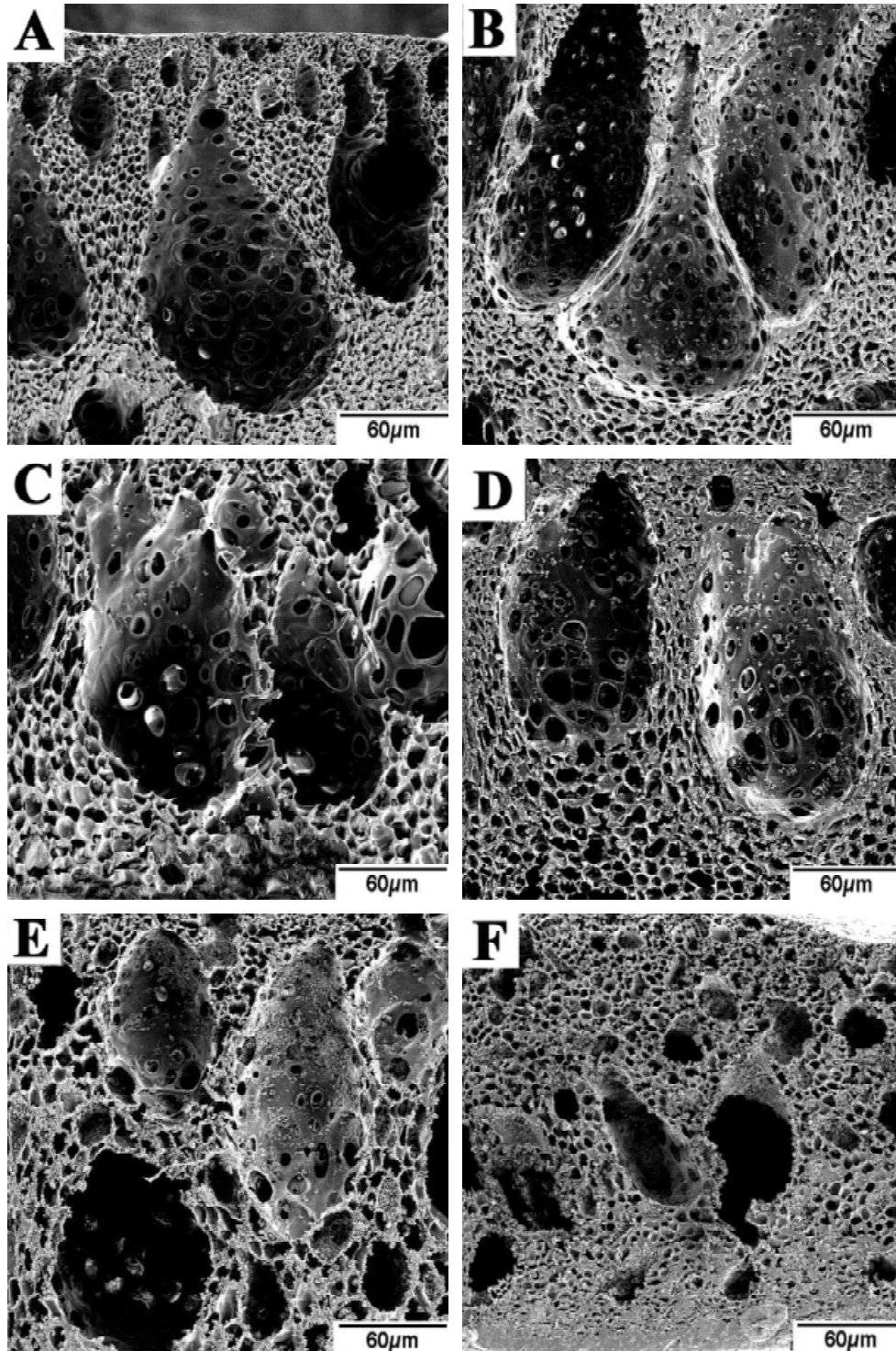


Figure 2. Cross-section SEM images of (A) porous polysulfone (PS7) and porous polysulfone/bioactive glass composites: (B) PS3; (C) PS4; (D) PS1; (E) PS5; (F) PS6.

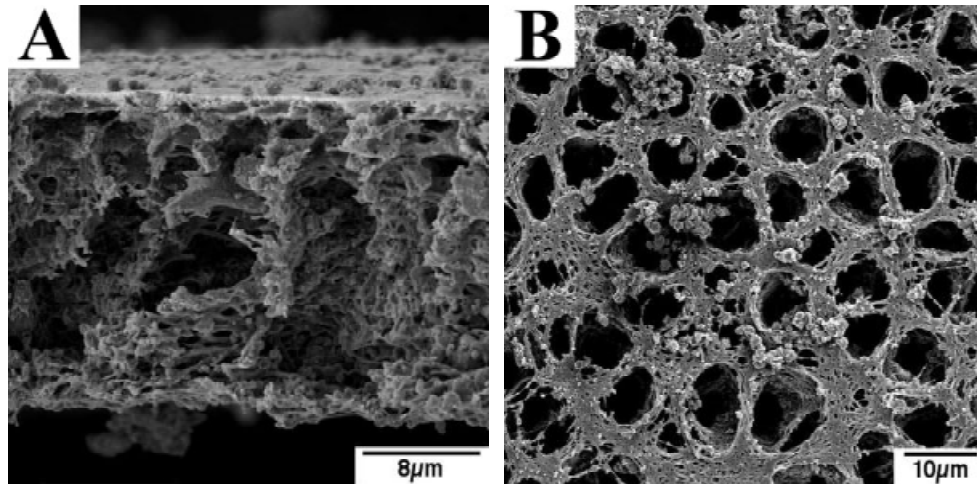


Figure 3. SEM images of porous cellulose acetate/bioactive glass composite (CA1): (A) cross-section; (B) bottom surface.

glass content, which has smaller large voids compared to the other composites. Mercury porosimetry data showed that the total pore content did not vary much. The polysulfone material without glass (PS7) has a porosity of 73.3 volume%, whereas PS1 was 71.3%, PS5 was 76%, and PS6 was 69.0%.

SEM images of the cross-section and the bottom surface of a cellulose acetate/bioactive glass composite (CA1) are shown in Figure 3. The microstructure is similar to the polysulfone-based composites with larger voids and smaller voids; however, the larger voids are narrower and extend more completely through the thickness. The microstructure of these composites was more sensitive to the dispersion composition. For example, CA3 has a higher glass content and a much less porous microstructure (see Fig. 4). The bottom surface shows that the diameters of large voids are about 10 times smaller than those in CA1. This change is similar to that observed by Androff et

al.³⁵ when the polymer adsorbs on the ceramic particles in the dispersion.

Past research on similar composites indicates the changes in microstructure are brought about when the polymer adsorbs on the ceramic particles in suspension.^{35, 36} Figure 5 shows the adsorption behaviors of both polymers on bioactive glass. With polymer adsorbed on their surfaces, ceramic particles become part of the polymer-rich phase during the phase separation and tend to be incorporated in the polymer-rich matrix. Increasing glass particle content increases the stiffness of the polymer-rich phase, which inhibits the formation of larger polymer lean regions and hence voids. Adsorption and suppression of large voids with increasing glass content was observed for cellulose acetate/bioactive glass composites.

In the case of polysulfone/bioactive glass, the polymer does not adsorb as strongly, likely due to its more hydrophobic character. During phase separation, the

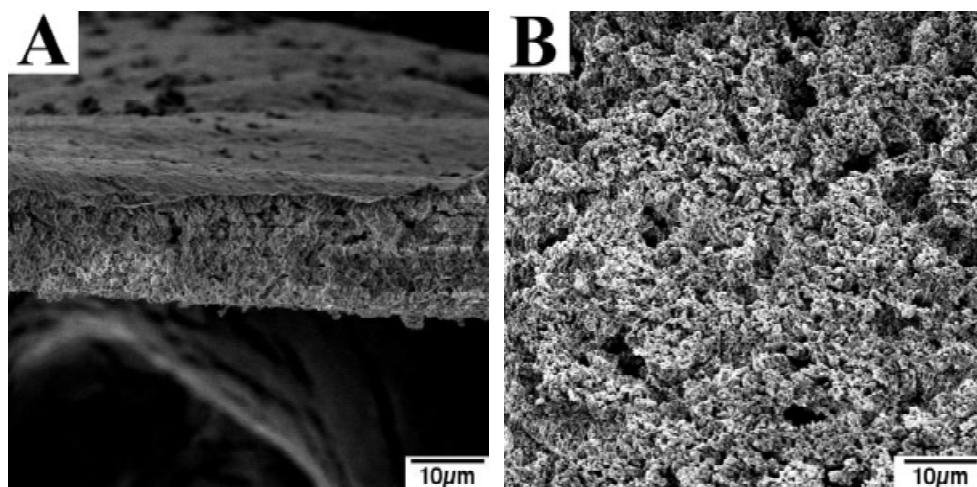


Figure 4. SEM images of porous cellulose acetate/bioactive glass composite (CA3): (A) cross-section; (B) bottom surface.

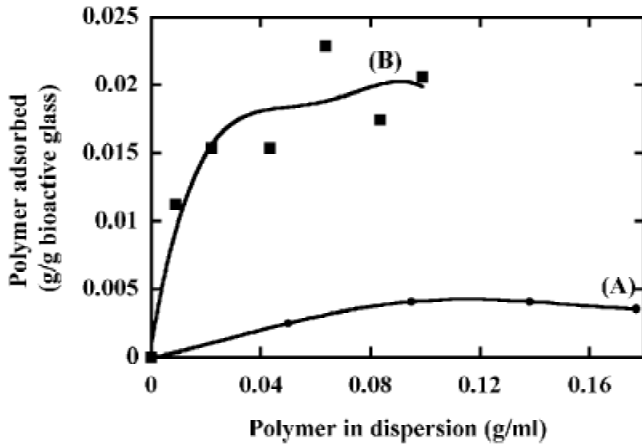


Figure 5. Adsorption isotherms of (A) polysulfone and (B) cellulose acetate on bioactive glass particles in dispersions.

glass particles are not as likely to be segregated to the polymer-rich phase and hence do not influence the pore structure development as much. However, particles are entrapped in the polymer rich phase during phase separation, and the void structure at higher loadings of glass does change (see Fig. 2), indicating that the glass is playing a role in the development of structure.

The dense layers on the top and bottom surfaces of the composites present a challenge to their future application as interface materials, as these layers can serve as a barrier for cell in-growth, nutrient transportation and bonding to tissues. One practical method to remove these dense layers is abrading their surfaces to expose the inner porous structure. An SEM image of an abraded polysulfone/bioactive glass composite is shown in Figure 6. Large pores with a size over 100 μm were exposed after the abrasion. A promising alternative method of creating surface pores involves

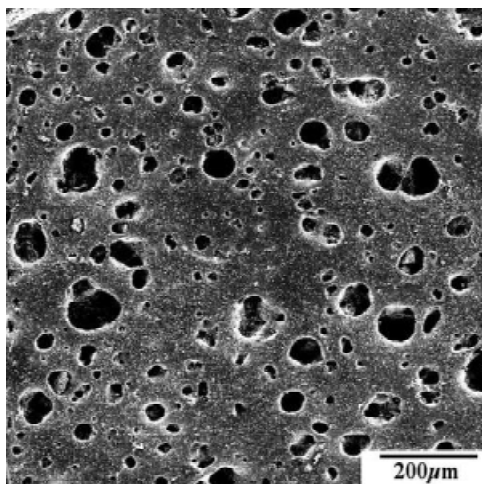


Figure 6. SEM image of the surface of an abraded porous polysulfone/bioactive glass composite (PS1).

salt leaching from the surface; a study is currently underway and will be reported separately.

Hydroxycarbonate apatite growth

Figure 7 shows the SEM images of polysulfone/bioactive glass composites (PS1, without abrasion) after soaking in SBF for 2 weeks. In comparison to before soaking (see Fig. 1), the surfaces of the composite and the morphology of the glass particles distributed in the polysulfone matrix are different. A flake-like structure developed on the surface of the particles but not on the polysulfone matrix surface inside the composite. The bottom surface [Fig. 7(c,d)] shows a layer of new material composed of micron-sized clusters with a fine texture. The top surface of the composite was also modified in a similar way, but the new material did not cover the surface completely.

Figure 8 shows the morphology of an abraded polysulfone/bioactive glass composite (PS1) after soaking in SBF for 2 weeks. In this composite, flake-like material was found inside the composite not only on the glass particles, but also on the polysulfone matrix. The formation of apatite throughout the structure indicates that simulated body fluid permeated the structure and that the pores are interconnected. Similar material also developed on both bottom and top surfaces of abraded composites, forming a sheet-like structure; however, the openings of the large pores were not covered by this new material.

Similar results also obtained for the cellulose acetate/bioactive glass composites after two weeks of soaking in SBF. Figure 9 shows the microstructure of a composite (CA2) after soaking. Material with a flake-like structure was found on the top and bottom surfaces and inside the composites. All of the exposed porosity remained open after soaking. A composite with a denser surface structure (CA4) showed a continuous layer of new material after soaking; however, inside the composite new material forms on particles and on the matrix. Of note in comparison with the structure of polysulfone-based composites is that the cellulose acetate composites have higher glass content and the polymer is more hydrophilic than polysulfone.

Figure 10 shows the XRD patterns of polysulfone/bioactive glass composites (PS1, not abraded) after soaking in the SBF for 2 weeks. The composite was mounted so that its bottom surface was analyzed. Before soaking, the composite is amorphous. After soaking for 2 weeks in the SBF, apatite peaks (JCPDS 9-0432) were observed, showing that the new material observed on the composites is crystalline apatite. The FTIR-DRIFTS (diffuse reflectance mode) pattern for the flake-like material removed from the same polysulfone/bioactive glass composite sample is shown in

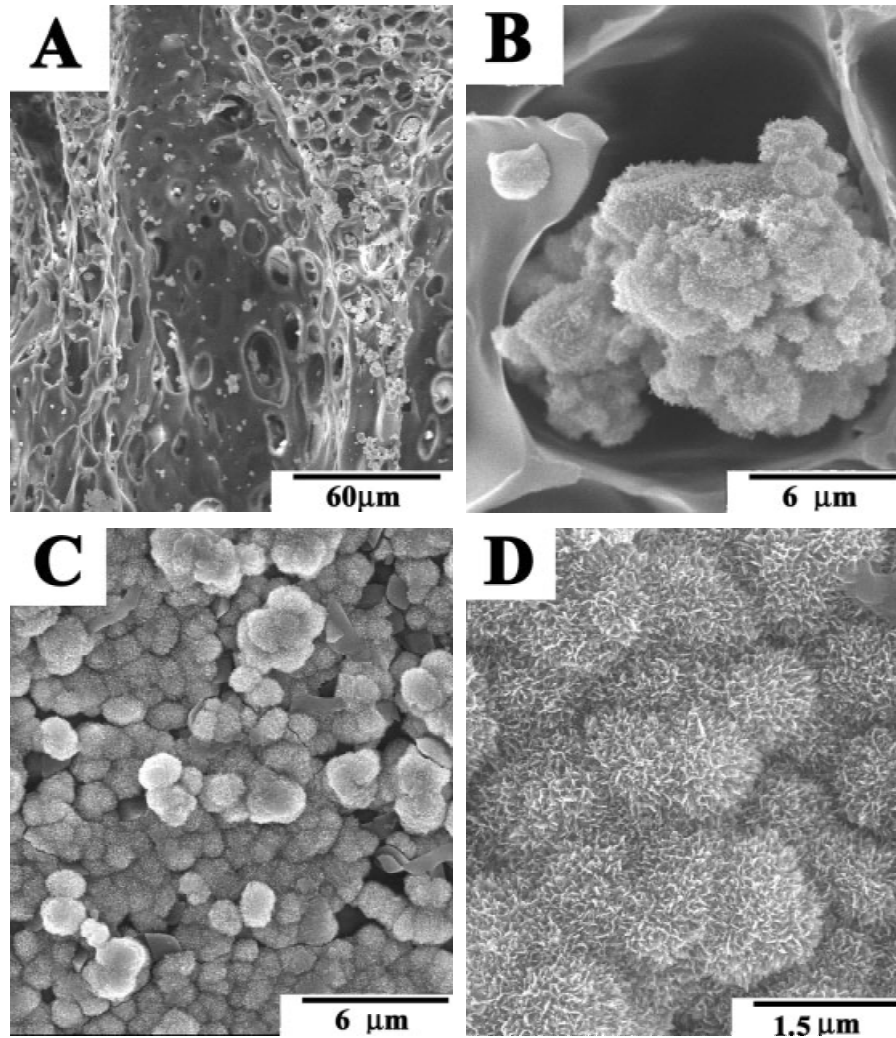


Figure 7. SEM images of nonabraded polysulfone/bioactive glass composite (PS1) after soaking in SBF for 2 weeks: (A) cross-section, 500 \times ; (B) cross-section, 5000 \times ; (C) bottom surface, 5000 \times ; and (D) bottom surface, 20000 \times .

Figure 11. The characteristic bands for phosphate group (472, 565, 604, 962, and 1035 cm^{-1}) and carbonate group (873, 1419, and 1456 cm^{-1})^{39,40} were observed, showing that the new material in the composite is HCA. Likewise, apatite was detected for abraded polysulfone-based composites and the cellulose acetate-based composites that were soaked in SBF.

No apatite was developed either for the pure porous polysulfone or cellulose acetate materials after soaking in SBF for 2 weeks.

The mechanism for the formation of bonelike apatite on bioactive glasses after soaking in SBF has been well-studied.^{38,41,42} The HCA formation mechanism on A/W glass and glass-ceramics proposed by Kokubo^{43,44} can be generalized by three steps: (1) release of calcium ions from the glass, increasing of ion activity product of the apatite in the surrounding body fluid; (2) apatite nucleation on hydrated silica sites on the surface of the glass; and (3) growth of apatite by consumption of calcium and phosphate ions from the

surrounding body fluid. Based on this mechanism, Tanahashi et al.⁴⁵ developed a method to form bone-like apatite on dense polymers. The polymer undergoes an apatite nucleation step in the presence of bioactive glass and SBF, followed by an apatite growth step in a more concentrated SBF.⁴⁵ (Apatite forms on some hydrophilic polymers directly on soaking in SBF and similar fluids.^{46,47}) The importance of the presence of bioactive glass for developing HCA has also been shown by formation of apatite on dense polysulfone/bioactive glass fiber composites developed for orthopaedic applications.^{19,20} Likewise in the composites studied here, the bioactive glass was necessary for HCA formation in and on the porous polymer matrix. HCA did not form on the polymer matrices alone.

During the soaking of nonabraded polysulfone/bioactive glass composites, the supply of SBF into pores in the composites was hindered by the composites' denser outer surfaces and the apatite layers that formed on their surfaces. SEM studies show the outer

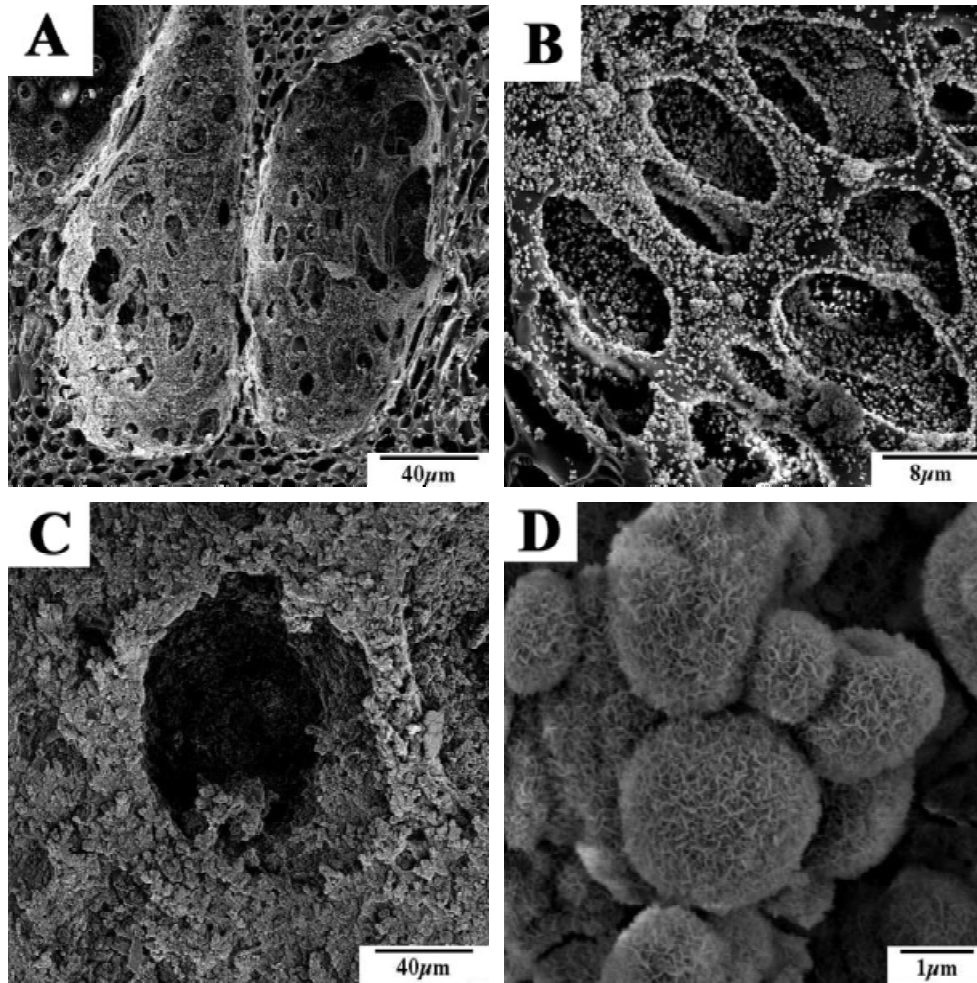


Figure 8. SEM images of abraded polysulfone/bioactive glass composite (PS1) after soaking in SBF for 2 weeks: (A) cross-section, 500 \times ; (B) cross-section, 2500 \times ; (C) bottom surface, 500 \times ; and (D) bottom surface 15000 \times .

surfaces covered with apatite while the interior had flake-like material on the glass alone. The formation of the apatite on the composite outer surface is likely due to the relatively small surface area (fewer nucleation sites) and the plentiful supply of ions for growth. These results are consistent with those of Zhang and Ma,⁴⁶ which show that the rate and amount of HCA formation for a dense poly(L-lactic acid) sample were higher than those for a porous poly(L-lactic acid) when soaked in a modified SBF. When the polysulfone/bioactive glass composite surfaces were abraded, the porous internal structure was exposed and the SBF had better access to the inside of the composites. In this case, apatite formed on the inside the composites (on glass and on the polysulfone matrix surface) as well as on the outer surface. Another possible reason for more apatite formation in the abraded composites may be that the surface treatment in ethanol before soaking in SBF induced polar groups onto the composites' surfaces. Ethanol was used to wet the composites' matrix surfaces and the residual polar hydroxyl group on the polymer surface

may trap silicate ions and help the apatite nucleation.^{44,48-51}

Compared with the nonabraded polysulfone/bioactive glass composites, more HCA grew inside the cellulose acetate/bioactive glass composites even though the composite had a dense top layer and small bottom pores. The larger bioactive glass content in these composites is an important factor contributing to the differences. In addition, carboxylic acid groups, developed from hydrolysis of cellulose acetate, result in negatively charged carboxylate anions which may provide apatite nucleation sites.⁴⁶ However, the bioactive glass was still necessary for apatite formation in cellulose acetate.

Previous research has correlated the ability of biomaterials to develop HCA upon soaking in SBF relates to bone bonding *in vivo*.^{52,53} Therefore, the *in vitro* formation of HCA in polysulfone/bioactive glass composites after soaking in SBF demonstrates their bone bonding ability. Studies on the interaction between composites and chondrocytes in culture are underway and will be reported separately.

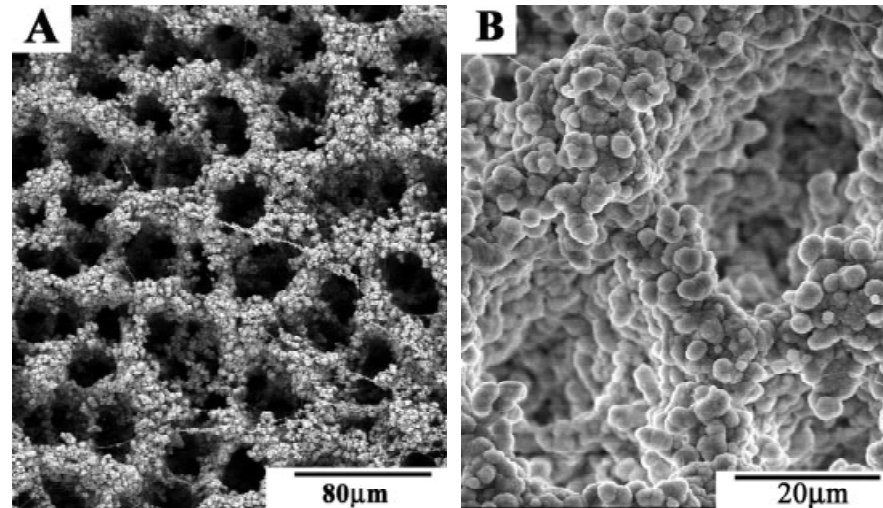


Figure 9. SEM images of bottom surface of cellulose acetate/bioactive glass composite (CA2) after soaking in SBF for 2 weeks: (A) 350 \times , backscattered image which highlights glass particles; (B) 1500 \times .

Mechanical properties

The mechanical properties of porous polysulfone and porous polysulfone/bioactive glass composites are shown in Figures 12 and 13. Representative tensile test data (Fig. 12) show an elastic region at low levels of force, followed by plastic deformation and failure. The composites are stiffer and stronger than the polymer alone, as shown also in Figure 13. The elastic modulus of the composites increases significantly with the addition of bioactive glass, which has a higher modulus than the polymer. In dense composites, experimental^{54,55} and modeling^{55–57} studies show that the addition of higher modulus glass or ceramic particles to a polymer matrix increases its modulus. In porous composites, however, pore structure and content affect the modulus in addition to the relative amounts of glass and polymer. Decoupling the effects

of glass and pore content requires a model that accounts for both variables.

One approach is to start with a model that accounts for the effect of porosity on the elastic modulus of a highly porous material, such as foam, given by the following expression:

$$E = E_o (1 - P)^n \quad (1)$$

where E_o is the modulus of the solid phase (without pores), P is the pore fraction and n is a constant that depends on the microstructure.⁵⁸ When the experimental data for E and P of porous polysulfone (PS7) are inserted into Eq (1) along with the reported modulus of dense polysulfone (E_o) 2482 MPa,²⁸ the constant n is found to be 1.88. This value is close to 2, the theoretically predicted value for open cell foams.⁵⁸ For the composites in this study, E_o depends on the amount of glass incorporated into the polymer matrix.

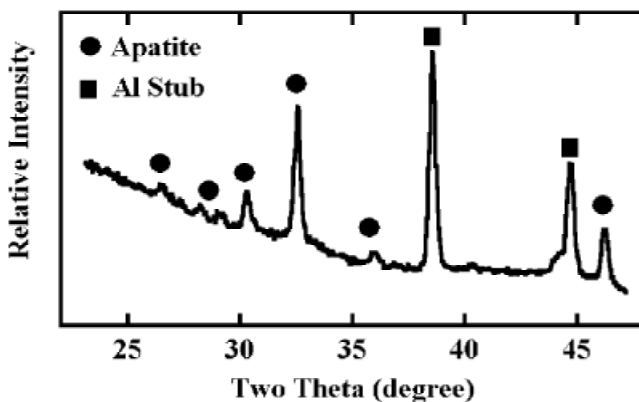


Figure 10. XRD data for nonabraded polysulfone/bioactive glass composite (PS1) after soaking in SBF for 2 weeks.

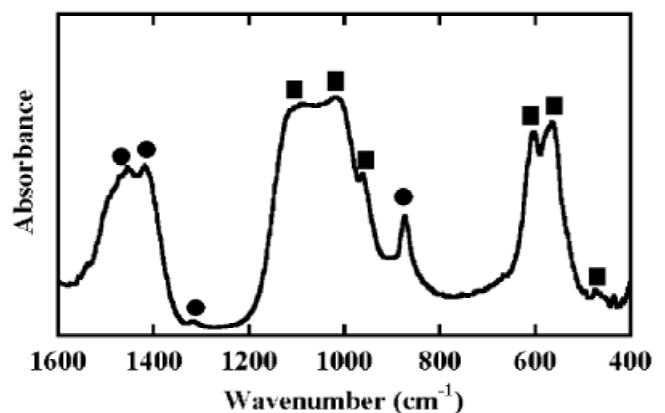


Figure 11. FTIR spectrum of the new material on the non-abraded polysulfone/bioactive glass composite (PS1) after soaking in SBF for 2 weeks. Characteristic absorbances for phosphate (■) and carbonate (●) are shown.

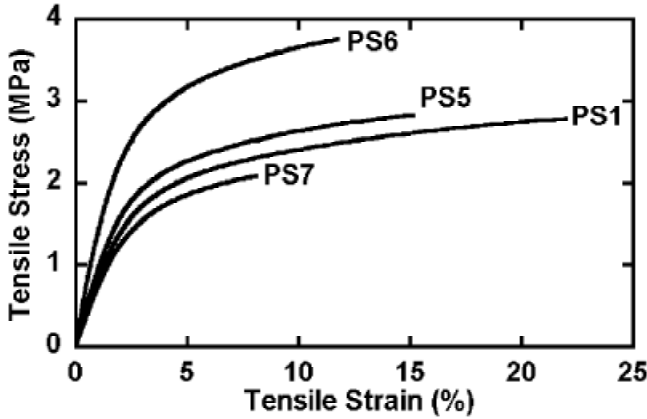


Figure 12. Representative tensile test data for porous polysulfone (PS7) and porous polysulfone/bioactive glass composites (PS1, PS5, PS6); specimens were abraded to remove dense surfaces before testing. Data collected using a dynamic mechanical analyzer (DMA) with static stress mode (loading rate: 500 mN/min).

Using a model developed by Ishai and Cohen,⁵⁹ the modulus of a dense composite, E_o in the context of this article, is:

$$E_o = E_P \left(1 + \frac{v_F}{m/(m-1) - v_F^{1/3}} \right) \quad (2)$$

where E_P is the modulus of the polymer (2482 MPa), m is the ratio of the modulus of the glass to that of the polymer (in this case $m = 36$, using 89 GPa for the modulus of the glass⁶⁰) and v_F is the volume fraction of glass incorporated into the polymer matrix (relative to the volume of the polymer and the incorporated glass). In terms of the porous composite volume,

$$v_F = \frac{v_{G1}}{v_{G1} + (1 - P - v_T)} \quad (3)$$

where v_{G1} is the volume fraction of glass incorporated into the polymer matrix (relative to the porous composite volume) and v_T is the total volume fraction of glass (relative to the porous composite volume). SEM results show that glass is both incorporated in the polymer matrix and on the pore surfaces; glass on the pore surfaces does not add to the modulus of the matrix, but rather behaves more like pores, filling space but not supporting a load. Hence, the pore fraction is

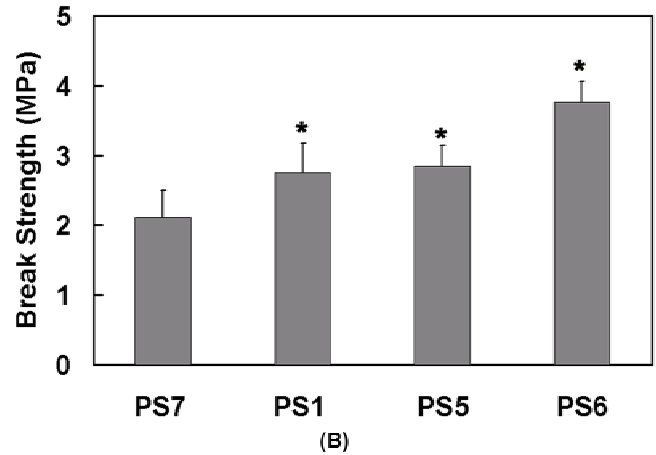
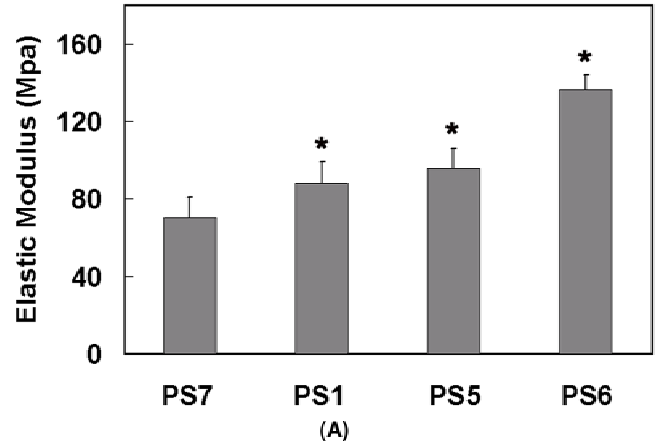


Figure 13. Variation of (A) elastic modulus and (B) break strength of porous polysulfone (PS7: average porosity = 85%) and porous polysulfone/bioactive glass composites (PS1: 9.4 vol% glass relative to total solids, average porosity = 83%; PS5: 20.4 vol% glass relative to total solids, average porosity = 81%; PS6: 29.2 vol% glass relative to total solids, average porosity = 74%). All materials had their denser top surfaces removed by abrasion. Data are shown for the average of nine specimens with bars showing one standard deviation and * indicating statistical difference compared to PS7 ($p < 0.05$).

in this case the sum of the measured pore fraction (P) and v_{G2} , the fraction of the glass that is not incorporated into the polymer matrix (relative to the porous composite volume). Thus, $v_T = v_{G1} + v_{G2}$. Therefore, Eq. (1) becomes:

$$E = E_o(1 - P - v_{G2})^n \quad (4)$$

TABLE III
Predictions of Glass Incorporated^a into the Polymer Matrix and Matrix Modulus

	V_T	p^b	E^c (MPa)	V_{G1}	V_{G2}	V_F	E_o (MPa)
PS1	0.016	0.83	88.0	0.0085	0.0075	0.052	2676
PS5	0.039	0.81	95.5	0.014	0.025	0.085	2840
PS6	0.076	0.74	136.2	0.016	0.060	0.080	2812

^aSee text for definitions.

^bDetermined from bulk density measurements of composites.

^cAverage from DMA analysis.

By combining Eq. 2–4 and assuming $E_p = 2482$ MPa, $n = 1.88$, $m = 36$, v_{G1} can be predicted for each composite (see Table III). The results show that the amount of glass incorporated into the polymer matrix is less than that in the porous composite as a whole (v_T). Nonetheless, calculations of E_c demonstrate that the presence of the glass increases the modulus of the composite matrix. The amount of glass incorporated in the polymer levels out and the amount segregated to the pores increases as more glass is added during processing, which may be due to the lack of strong adsorption of the polymer on the ceramic (see Fig. 5). These calculations provide a start to understanding the complex mechanical behavior of porous composites, but clearly more work is needed in this area. To develop a better model, finite element analysis methods such as those developed by Guild and Bonfield^{56,57} are required. In addition, experimental results from composites with varying pore content and constant glass content will be important for testing the model's validity.

The break strengths of the composites are higher than that of porous polysulfone. The enhancement is due, at least in part, to the increase in modulus. The composite with the highest glass content (PS6) is significantly stronger than the other materials. Since failure is likely initiated at the larger voids, the decrease in the size of the larger voids for this composite accounts for its higher strength. In dense polysulfone/bioglass® composites, decreased strength with increased glass content was observed because the particles themselves act as the critical flaws.⁶¹ More research is needed to balance the mechanical properties with the desired microstructural features for these porous composites.

CONCLUSIONS

Porous composites consisting of polysulfone (or cellulose acetate) and bioactive glass particles were produced by phase separation techniques. The composites have asymmetric structures with dense top layers and porous structures beneath. The dense top layer could be removed by abrasion to make a structure with large pores (20–150 μm) exposed. Microstructure control depends mainly on the choice of polymer and particularly in the case of a polymer that absorbs on the glass, the bioactive glass content. HCA growth inside and on the composites after soaking them in SBF suggests the bone-bonding ability of the composites. The pore content as well as the glass content affects the mechanical properties of the composites. These porous composites have potential applications as interfacial materials between soft and hard tissues, such as the artificial cartilage/bone interface.

We are grateful to Prof. T. R. Oegema, Jr., Prof. R. F. Cook, Dr. Hongwei Yan, Mary E. Grimm, Jiakuan Sun, and Jaime Grunlan for insightful discussions.

References

1. Millington PF. Cartilage–bone interface. *Eng Med* 1984;13:133–136.
2. Pashley DH. Dynamics of the pulpo–dentin complex. *Crit Rev Oral Biol Med* 1996;7:104–133.
3. Raspanti M, Strocchi R, De Pasquale V, Martini D, Montanari C, Ruggeri A. Structure and ultrastructure of the bone/ligament junction. *It J Anat Embryol* 1996;101:97–105.
4. Oegema TR Jr, Carpenter RJ, Hofmeister F Jr, Thompson RC. The interaction of the zone of calcified cartilage and subchondral bone in osteoarthritis. *Microscopy Res Techn* 1997;37:324–332.
5. Langer R, Vacanti JP. Tissue engineering. *Science* 1993;260:920–925.
6. Newman AP. Current concepts: articular cartilage repair. *Am J Sports Med* 1998;26:309–324.
7. Minas T, Nehrer S. Current concepts in the treatment of articular cartilage defects. *Orthopedics* 1997;20:525–538.
8. Buckwalter JA, Mankin HJ. Articular cartilage: part I: tissue design and chondrocyte–matrix interactions. *J Bone Joint Surg* 1997;79:600–611.
9. Buckwalter JA, Mankin HJ. Articular cartilage: part II: degeneration and osteoarthritis, repair, regeneration, and transplantation. *J Bone Joint Surg* 1997;79:612–632.
10. Caplan AI, Elyaderani M, Mochizuki Y, Wakitani S, Goldberg VM. Principles of cartilage repair and regeneration. *Clin Orthopaed Rel Res* 1997;342:254–269.
11. Brittberg M. Autologous chondrocyte transplantation. *Clin Orthopaed Rel Res* 1999;367S:S147–S155.
12. LeBaron RG, Athanasiou KA. Ex vivo synthesis of articular cartilage. *Biomaterials* 2000;21:2275–2587.
13. Vacanti CA, Vacanti JP. Bone and cartilage reconstruction. In: Lanza RP, Langer R and Chick WL, editors. *Tissue engineering*. San Diego, CA: Academic Press; 1995. p 619–631.
14. Grande DA, Breitbart AS, Mason J, Paulino C, Laser J, Schwartz RE. Cartilage tissue engineering: current limitations and solutions. *Clin Orthopaed Rel Res* 1999;367S:S176–S185.
15. Huntmacher DW. Scaffolds in tissue engineering bone and cartilage. *Biomaterials* 2000;21:2529–2543.
16. Kandel RA, Boyle J, Gibson G, Cruz T, Speagle M. *In vitro* formation of mineralized cartilaginous tissue by articular chondrocytes. *In Vitro Cell Dev Biol* 1997;33:174–181.
17. Hench LL. Bioceramics. *J Am Ceram Soc* 1998;1705–1728.
18. Loty C, Forest N, Boulekbache H, Kokubo T, Sautier JM. Behavior of fetal rat chondrocytes cultured on a bioactive glass-ceramic. *J Biomed Mater Res* 1997;37:137–149.
19. Marcolongo M, Ducheyne P, LaCourse WL. Surface reaction layer formation in vitro on a bioactive glass fiber/polymeric composite. *J Biomed Mater Res* 1997;37:440–448.
20. Marcolongo M, Ducheyne P, Garino J, Schepers E. Bioactive glass fiber/ polymeric composites bond to bone tissue. *J Biomed Mater Res* 1998;39:161–170.
21. Wang M, Hench LL, Bonfield W. Bioglass/high density polyethylene composite for soft tissue applications: Preparation and evaluation. *J Biomed Mater Res* 1998;42:577–586.
22. Zhang K, Francis LF. In: *Transactions of the 27th Annual Meeting of the Society for Biomaterials*, St. Paul, MN, 2001.
23. Ma PX, Langer R. Morphology and mechanical function of long-term in vitro engineered cartilage. *J Biomed Mater Res* 1999;44:217–221.

24. Göpferich A. Mechanisms of polymer degradation and erosion. *Biomaterials* 1996;17:103–114.
25. Spector M, Michno MJ, Smarook WH, Kwiatkowski GT. A high-modulus polymer for porous orthopedic implants: biomechanical compatibility of porous implants. *J Biomed Mater Res* 1978;12:665–677.
26. Zdrahala RJ, Zdrahala I. Biomedical application of polyurethanes: a review of past promises, present realities, and a vibrant future. *J Biomater Appl* 1999;14:67–90.
27. Messner K. Durability of artificial implants for repair of osteochondral defects of the medial femoral condyle in rabbits. *Biomaterials* 1994;15:657–664.
28. Dickinson BL. UDEL® Polysulfone for medical applications. *J Biomater Appl* 1989;3:605–634.
29. Pesek SC, Koros WJ. Aqueous quenched asymmetric polysulfone membranes prepared by dry/wet phase separation. *J Membrane Sci* 1993;81:71–88.
30. Hench LL, Splinter RJ, Allen WC, TK Greenlee Jr. Bonding mechanisms at the interface of ceramic prosthetic materials. *J Biomed Mater Res* 1971;2:117–141.
31. Kokubo T, Shigematsu M, Nagashima Y, Tashiro M, Yamamuro T, Higashi S. Apatite-and Wollastonite-containing glass-ceramics for prosthetic application. *Bull Inst Chem Res* 1982;60:260–268.
32. Wilson J, Pigott GH, Schoen FJ, Hench LL. Toxicology and biocompatibility of bioglass. *J Biomed Mater Res* 1981;15:805–817.
33. Wilson J, Nolletti D. Bonding of soft tissues to bioglass. In: Yamamuro T, Hench LL and Wilson J, editors. *Handbook on bioactive ceramics: bioactive glasses and glass-ceramics*, Vol. I. Boca Raton, FL: CRC; 1990. p 283–302.
34. Sautier JM, Kokubo T, Ohtsuki T, Nefussi JR, Boulekbache H, Oboeuf M, Loty S, Loty C, Forest N. Bioactive glass-ceramic containing crystalline apatite and wollastonite initiates biomineralization in bone cell cultures. *Calcif Tissue Int* 1994;55:458–466.
35. Androff NM, Francis LF, Velamakanni BV. Macroporous ceramics from ceramic-polymer dispersion methods. *AIChE J* 1997;43:2878–2888.
36. Wara NM. Processing of macroporous ceramics through ceramic-polymer dispersion methods. Ph.D. Thesis, University of Minnesota, 1996.
37. Pinnau I, Koros WJ. A qualitative skin layer formation mechanism of membranes made by dry/wet phase inversion. *J Polym Sci: Part B* 1993;31:419–427.
38. Kokubo T, Kushitani H, Ohtsuki C, Sakka S, Yamamuro T. Chemical reaction of bioactive glass and glass-ceramics with a simulated body fluid. *J Mater Sci* 1992;1:233–238.
39. Rehman I, Bonfield W. Characterization of hydroxyapatite and carbonated apatite by photo acoustic FTIR spectroscopy. *J Mater Sci* 1997;8:1–4.
40. Kim H, Rey C, Glimcher MJ. X-Ray diffraction, electron microscopy, and Fourier transform infrared spectroscopy of apatite crystals isolated from chicken and bovine calcified cartilage. *Calcif Tissue Int* 1996;59:58–63.
41. Ohtsuki C, Kokubo T, Yamamuro T. Mechanism of apatite formation on CaO–SiO₂–P₂O₅ glasses in a simulated body fluid. *J Non-Cryst Solids* 1992;143:84–92.
42. Li P, Ohtsuki C, Kokubo T, Nakanishi K, Soga N, Nakamura T, Yamamuro T. Apatite formation induced by silica gel in a simulated body fluid. *J Am Ceram Soc* 1992;75:2094–2097.
43. Kokubo T. A/W Glass-ceramic: Processing and properties. In: Hench LL and Wilson J, editor. *Bioceramics*. Singapore: World Scientific; 1993. p 75–88.
44. Kokubo T. Apatite formation on surfaces of ceramics, metals and polymers in body environment. *Acta Mater* 1998;46:2519–2527.
45. Tanahashi M, Yao T, Kokubo T, Minoda M, Miyamoto T, Nakamura T, Yamamuro T. Apatite coating on organic polymers by a biomimetic process. *J Am Ceram Soc* 1994;77:2805–2808.
46. Zhang R, Ma PX. Porous poly(L-lactic acid)/apatite composites created by biomimetic process. *J Biomed Mater Res* 1999;45:285–293.
47. Murphy W, Kohn DH, Mooney DJ. Growth of continuous bonelike mineral within porous poly(lactide-co-glycolide) scaffold *in vitro*. *J Biomed Mater Res* 2000;50:50–58.
48. Tanahashi M, Kokubo T, Minoda M, Miyamoto T, Nakamura T, Yamamuro T. Apatite coated on organic polymers by a biomimetic process: Improvement in its adhesion to substrates by NaOH treatment. *J Appl Biomater* 1994;5:339–347.
49. Tanahashi M, Yao T, Kokubo T, Minoda M, Miyamoto T, Nakamura T, Yamamuro T. Apatite coated on organic polymers by a biomimetic process: Improvement in its adhesion to substrates by glow discharge treatment. *J Biomed Mater Res* 1995;29:349–358.
50. Tanahashi M, Kokubo T, Minoda M, Miyamoto T, Nakamura T, Yamamuro T. Apatite coated on organic polymers by a biomimetic process: Improvement in its adhesion to substrates by HCl treatment. *J Mater Sci* 1995;6:319–326.
51. Larsen MJ, Thorsen A, Jensen SJ. Ethanol-induced formation of solid calcium phosphates. *Calcif Tissue Int* 1985;37:189–193.
52. Kokubo T. Bonding mechanism of bioactive glass-ceramic A-W to living bone. In: Yamamuro T, Hench LL and Wilson J, editors. *Handbook on bioactive ceramics: Bioactive glasses and glass-ceramics*, Vol. I. Boca Raton, FL: CRC; 1990. p 41–50.
53. Kokubo T, Kushitani H, Sakka S, Kitugi T, Yamamuro T. Solutions able to reproduce *in vivo* surface-structure changes in bioactive glass-ceramic A-W. *J Biomed Mater Res* 1990;24:721–734.
54. Spanaoudakis, J, Young RJ. Crack propagation in a glass particle-filled epoxy resin Part 2 effect of particle-matrix adhesion. *J Mater Sci* 1984;19:487–96.
55. Ahmed S, Jones FR. A review of particulate reinforcement theories for polymer composites. *J Mater Sci* 1990;25:4933–4942.
56. Guild FJ, Bonfield W. Predictive modelling of hydroxyapatite-polyethylene composite. *Biomaterials* 1993;14:985–94.
57. Guild FJ, Bonfield W. Predictive modelling of mechanical properties and failure processes in hydroxyapatite-polyethylene (Hapex™) Composite. *J Mater Sci* 1998;9:496–502.
58. Gibson LJ and Ashby MF. *Cellular Solids Structure and Properties*. Elmsford, NY: Pergamon Press, Inc.; 1988. p 120–168.
59. Ishai O, Choen LJ. Elastic properties of filled and porous composites. *Int J Mech Sci* 1967;9:539–546.
60. Kokubo T, Ito S, Shigematsu M, Sakka S, Yamamuro T. Mechanical properties of a new type of apatite-containing glass-ceramic for prosthetic application. *J Mater Sci* 1985;20:2001–2004.
61. Orefice RL, LaTorre GP, West JK, Hench LL. Processing and characterization of bioactive polysulfone-bioglass® composites. In: Wilson J, Hench LL, Greenspan, D editors. *Bioceramics*, Vol. 8 Oxford: Alden Press; 1995. p. 409–414.